

Photon-dark photon conversion with multiple level crossings

Nirmalya Brahma,¹ Asher Berlin^{1,2,3,4} and Katelin Schutz¹

¹*Department of Physics and Trottier Space Institute, McGill University,
Montréal, Quebec H3A 2T8, Canada*

²*Theory Division, Fermi National Accelerator Laboratory, Batavia, Illinois 60510, USA*

³*Superconducting Quantum Materials and Systems Center (SQMS),
Fermi National Accelerator Laboratory, Batavia, Illinois 60510, USA*

⁴*Perimeter Institute for Theoretical Physics, Waterloo, Ontario N2L 2Y5, Canada*



(Received 11 September 2023; accepted 3 November 2023; published 28 November 2023)

Dark photons can oscillate into Standard Model (SM) photons via kinetic mixing. The conversion probability depends sensitively on properties of the ambient background, such as the density and electromagnetic field strength, which cause the SM photon to acquire an in-medium effective mass. Resonances can enhance the conversion probability when there is a level-crossing between the dark photon and background-dependent SM photon states. In this work, we show that the widely used Landau-Zener (LZ) approximation breaks down when there are multiple level-crossings due to a nonmonotonic SM photon potential. Phase interference effects, especially when the dark photon mass is close to an extremum of the SM photon effective mass, can cause deviations from the LZ approximation at the level of a few orders of magnitude in the conversion probability. We present an analytic approximation that is valid in this regime and that can accurately predict the conversion probabilities in a wide range of astrophysical environments.

DOI: [10.1103/PhysRevD.108.095045](https://doi.org/10.1103/PhysRevD.108.095045)

I. INTRODUCTION

Dark photons (DPs) are the gauge bosons of a hidden $U(1)'$ symmetry that may be spontaneously broken (analogous to the Higgs mechanism) or broken explicitly (with the Stueckelberg action for a spin-1 field), yielding a nonzero dark photon mass. In general, DPs will mix with Standard Model (SM) photons at some level via the dimension-4 kinetic mixing operator. The additional terms in the Lagrangian capturing the effects of the DP field A' mixing with the SM photon field A are

$$\mathcal{L} \supset -\frac{1}{4}F'_{\mu\nu}F'^{\mu\nu} + \frac{\epsilon}{2}F'_{\mu\nu}F^{\mu\nu} + \frac{1}{2}m_{A'}^2 A'_\mu A'^\mu, \quad (1)$$

where F' and F are the dark and SM field strength tensors, $\epsilon \ll 1$ is the dimensionless coupling that determines the strength of kinetic mixing with the SM photon, and $m_{A'}$ is the DP mass. Kinetic mixing has attracted considerable interest as a portal to dark sectors that would be accessible at a wide range of energies since it is a marginal operator. In particular, ϵ could be generated by any number of mechanisms [1–11], for instance by loop diagrams with heavy

matter fields charged under both $U(1)'$ and the SM $U(1)$, or alternatively from certain realizations of string theory. From a bottom-up effective field theory point of view, ϵ can be thought of as a free parameter accompanying a marginal operator.

Astrophysical and cosmological observations provide some of the tightest constraints on the existence of DPs over a wide range of masses [12–21]. These constraints often involve oscillations between DPs and SM photons leading to spectral imprints or new energy loss mechanisms. Furthermore, this conversion is resonantly enhanced if there is an energy level-crossing due to in-medium contributions to the SM photon effective mass. Large corrections to the SM photon mass arise from ambient free charges or strong background electromagnetic fields [22,23], and corrections to the DP effective mass can also arise due to a background of dark sector particles directly charged under the DP [24,25].

In-medium effective masses can vary considerably over spatial or temporal domains in astrophysical and cosmological environments. In the case of nonadiabatic transitions due to a level-crossing, the conversion probability is usually well-approximated by the Landau-Zener (LZ) formula [26,27], which is often employed in such calculations as the leading-order term in the stationary phase approximation. However, this formalism breaks down when applied to the special case of resonant conversions occurring near local minima or maxima of the SM photon's

Published by the American Physical Society under the terms of the Creative Commons Attribution 4.0 International license. Further distribution of this work must maintain attribution to the author(s) and the published article's title, journal citation, and DOI. Funded by SCOAP³.

in-medium mass (which can depend on the photon frequency). This breakdown therefore occurs generically in environments where the density of SM particles is non-monotonic in space or time as traversed by SM photons. The conversion probability predicted by the LZ formula can deviate from the full solution to the Schrödinger equation (to leading order in ϵ) by several orders of magnitude. Therefore, there may be regions of DP parameter space at specific masses where existing constraints are subject to large corrections. In this work, we provide a simple analytic expression, Eq. (25), that is more generally applicable to this region of parameter space and discuss the potential impact on DP oscillation probabilities. We note that although we concretely work with DP oscillations in this paper, the formalism developed here can potentially be applied to axion-photon conversions as well as neutrino oscillations.

The rest of this paper is organized as follows. In Sec. II, we review various formalisms for computing transition probabilities for two-state systems. In Sec. III, we quantify the breakdown of the LZ approximation near the critical mass with an illustrative toy example. In Sec. IV, we examine the consequences of the breakdown of the LZ approximation in a few case examples arising in astrophysical and cosmological settings, such as neutron star magnetospheres and the solar chromosphere, as well as during the epoch of reionization. Concluding remarks follow in Sec. V.

II. PHOTON-DARK PHOTON OSCILLATION FORMALISM

A. Photon-dark photon oscillations in an arbitrary in-medium potential

The kinetic terms in Eq. (1) can be made canonical by moving to the active-sterile basis described by the A_a and A_s fields,

$$A^\mu \equiv \begin{pmatrix} A_a^\mu \\ A_s^\mu \end{pmatrix} = \begin{pmatrix} 1 & 0 \\ -\epsilon & 1 \end{pmatrix} \begin{pmatrix} A^\mu \\ A'^\mu \end{pmatrix} + \mathcal{O}(\epsilon^2), \quad (2)$$

to leading order in ϵ . Using this in Eq. (1), we then have

$$\begin{aligned} \mathcal{L} = & -\frac{1}{4} F_{\mu\nu}^a F_a^{\mu\nu} - \frac{1}{4} F_{\mu\nu}^s F_s^{\mu\nu} + e J_\mu A_a^\mu \\ & + \frac{1}{2} \mathbf{A}_\mu^T \begin{pmatrix} 0 & \epsilon m_{A'}^2 \\ \epsilon m_{A'}^2 & m_{A'}^2 \end{pmatrix} \mathbf{A}^\mu + \mathcal{O}(\epsilon^2), \end{aligned} \quad (3)$$

where $F_a^{\mu\nu}$ and $F_s^{\mu\nu}$ are the active and sterile field strengths and we have also included the coupling of A_a to the SM current density J . This basis is often referred to as the interaction basis, since SM currents selectively couple to the active state A_a . However, note that the mass matrix is nondiagonal in this case. As a result, although the sterile state is not sourced directly from SM currents, it arises

indirectly from $A_a \leftrightarrow A_s$ oscillations, which are the focus of this work.

In a medium, the free charges and electromagnetic fields in the background can source a potential that alters the dispersion relation of the active photons. We parametrize this effect by including a spatially dependent in-medium mass $m_{\text{eff}}(\mathbf{x})$ for the visible field A_a in Eq. (3). The in-medium mass-squared matrix is then given by

$$\mathcal{M}^2(\mathbf{x}) \simeq \begin{pmatrix} m_{\text{eff}}^2(\mathbf{x}) & \epsilon m_{A'}^2 \\ \epsilon m_{A'}^2 & m_{A'}^2 \end{pmatrix}. \quad (4)$$

In this section, we remain agnostic about the specific form of $m_{\text{eff}}(\mathbf{x})$, leaving an exploration of specific examples to Sec. IV.

We can track the propagation of the $A_a - A_s$ system by solving the corresponding equation of motion from Eqs. (3) and (4). Following Ref. [28], we switch to Fourier space, where ω and k are the frequency and wave number of the field A^μ , respectively, and assume that $m_{\text{eff}}(\mathbf{x})$ varies on scales much larger than k^{-1} . In this case, we can approximate this in-medium contribution as a constant on the scale of the de Broglie wavelength, such that the equation of motion for transverse modes takes the form of a standard wave equation,

$$[\omega^2 - k^2 - \mathcal{M}^2(\mathbf{x})] \mathbf{A}^\mu(\omega, k) = 0. \quad (5)$$

We note that an analogous dispersion relation of the form $(\omega^2 - \mathcal{M}_L^2) \mathbf{A}_L = 0$ holds for longitudinal modes, but a dedicated study of their evolution is beyond the scope of this work.

To proceed, we expand Eq. (5) in the relativistic limit $\omega \simeq k \gg m_{A'}, m_{\text{eff}}$ to obtain a linearized Schrödinger-like equation, as in Ref. [28]. We choose to work with the spatial domain marked by the position z , but can equivalently use the temporal domain since we deal with the propagation of relativistic particles in this work. This gives $i\partial_z \mathbf{A} = H \mathbf{A}$, where the total Hamiltonian $H = H_0 + H_1$ is split into diagonal and off-diagonal components,

$$H_0 = \begin{pmatrix} \omega + \Delta & 0 \\ 0 & \omega + \Delta_{A'} \end{pmatrix}, \quad H_1 = \begin{pmatrix} 0 & \epsilon \Delta_{A'} \\ \epsilon \Delta_{A'} & 0 \end{pmatrix}, \quad (6)$$

with

$$\Delta = -m_{\text{eff}}^2(z)/2\omega \quad \text{and} \quad \Delta_{A'} = -m_{A'}^2/2\omega. \quad (7)$$

Since $\epsilon \ll 1$, we can approximate $H_1 \ll H_0$ and use the techniques of time-dependent perturbation theory to solve for the evolution of \mathbf{A} . In particular, we switch to the interaction picture where $i\partial_z \mathbf{A}_{\text{int}} = H_{\text{int}} \mathbf{A}_{\text{int}}$, such that $\mathbf{A}_{\text{int}}(z) = \mathcal{U}^\dagger(z) \mathbf{A}(z)$, $H_{\text{int}} = \mathcal{U}^\dagger H_1 \mathcal{U}$, and \mathcal{U} is defined to be

$$U(z) = \exp \left[-i \int_{z_i}^z dz' H_0(z') \right], \quad (8)$$

such that z_i marks the point at which we fix our initial condition $\mathbf{A}(z_i) = \mathbf{A}_{\text{int}}(z_i)$. Hence, the system evolves as $\mathbf{A}_{\text{int}}(z) = e^{-i \int_{z_i}^z dz' H_{\text{int}}(z')} \mathbf{A}(z_i)$, which in the Schrödinger picture is equivalent to

$$\mathbf{A}(z) = e^{-i \int_{z_i}^z dz' H_0(z')} e^{-i \int_{z_i}^z dz' H_{\text{int}}(z')} \mathbf{A}(z_i). \quad (9)$$

The first factor of Eq. (9) is determined by the definition of H_0 in Eq. (6). To proceed, we evaluate H_{int} using the Baker-Campbell-Hausdorff identity,

$$H_{\text{int}} = \epsilon \Delta_{A'}(z) \begin{pmatrix} 0 & e^{i\Phi(z)} \\ e^{-i\Phi(z)} & 0 \end{pmatrix}, \quad (10)$$

where we have defined

$$\Phi(z) = \int_{z_i}^z dz' \Delta_{\text{osc}}(z'), \quad \Delta_{\text{osc}} = \Delta - \Delta_{A'}. \quad (11)$$

This form of H_{int} in Eq. (10) can be used in the second factor of Eq. (9), after expanding to $\mathcal{O}(\epsilon)$. Up to an irrelevant overall phase, this yields

$$\mathbf{A}(z) \propto \begin{pmatrix} 1 & -i\epsilon c_+ \\ -i\epsilon e^{i\Phi(z)} c_- & e^{i\Phi(z)} \end{pmatrix} \mathbf{A}(z_i) + \mathcal{O}(\epsilon^2), \quad (12)$$

where we defined $c_{\pm} = \int_{z_i}^z dz' e^{\pm i\Phi(z')} \Delta_{A'}(z')$.

The probability of conversion between active and sterile states is then given by the square of the off-diagonal elements in the above expression,

$$P_{A_a \leftrightarrow A_s} = \epsilon^2 \left| \int_{z_i}^z dz' \Delta_{A'}(z') e^{i\Phi(z')} \right|^2 + \mathcal{O}(\epsilon^3). \quad (13)$$

In vacuum, there is no in-medium contribution to the active photon, $\Delta = 0$, and the above integral can be performed analytically, yielding the standard result

$$P_{A_s \leftrightarrow A_a} = 4\epsilon^2 \sin^2(\Delta_{A'}(z - z_i)/2). \quad (14)$$

More generally, for $\epsilon \ll 1$ and $\Delta \neq 0$, one can numerically integrate Eq. (13) in order to calculate the in-medium conversion probability. In this case, the integrand in Eq. (13) is very oscillatory, making it difficult to achieve a high degree of numerical accuracy. Near resonances, however, it is possible to accurately approximate $P_{A_a \leftrightarrow A_s}$ analytically, as discussed in the next subsection.

B. Stationary-phase approximation and the Landau-Zener formula

While the integrand in Eq. (13) typically exhibits highly oscillatory behavior, it varies slowly near stationary points z_n , defined by $\Phi'(z_n) = 0$, where the ‘‘prime’’ corresponds to a spatial derivative. Since the phase varies slowly in this region of coordinate space, its contribution to the integral is not canceled out by other regions’ contributions, where oscillations tend to interfere destructively and average to zero. From Eq. (11), it is evident that these stationary points occur when the resonance condition holds, $\Delta = \Delta_{A'}$, analogous to level crossings induced by matter effects within the context of neutrino oscillations [29,30]. In this case, Eq. (13) can be evaluated analytically by use of the stationary-phase approximation, in which $\Phi(z')$ and $\Delta_{A'}(z')$ in the integrand are Taylor expanded to second and zeroth order around $z' \simeq z_n$, respectively. This gives

$$\begin{aligned} P_{A_a \leftrightarrow A_s} &\simeq \epsilon^2 \left| \sum_n \sqrt{A_n} e^{i\Phi(z_n) + i\sigma_n \pi/4} \right|^2 \\ &= \epsilon^2 \left(\sum_n A_n + 2 \sum_{n < m} \sqrt{A_n A_m} \cos \Phi_{nm} \right), \end{aligned} \quad (15)$$

where the sums are over all stationary points $z_n \in [z_i, z]$, and in the first and second lines we have defined

$$A_n = \frac{2\pi \Delta_{A'}^2(z_n)}{|\Phi''(z_n)|}, \quad \sigma_n = \text{sign}[\Phi''(z_n)], \quad (16)$$

and

$$\Phi_{nm} = \Phi(z_n) - \Phi(z_m) + (\pi/4)(\sigma_n - \sigma_m), \quad (17)$$

respectively, where from Eq. (11) we have $\Phi''(z_n) = \Delta'(z_n)$. In the second line of Eq. (15), the first term is simply the sum of individual probabilities from each resonance. The second term instead stems from the interference between two different resonances, which gives rise to what we will refer to below as *phase effects*. Such phase effects imprint oscillatory behavior into the conversion probability as a function of $m_{A'}$ and ω .

As shown schematically in Fig. 1, the conversion probability undergoes a large number of oscillations between any two resonances if $|\Phi_{nm}| \gg 2\pi$, or equivalently

$$\left| \int_{z_m(\omega)}^{z_n(\omega)} dz' \frac{m_{A'}^2 - m_{\text{eff}}^2(z', \omega)}{2\omega} \right| \gg 2\pi, \quad (18)$$

where we have been explicit in regards to the spatial and frequency dependence. In this case, small variations in frequency within an observed resolution bandwidth could lead to variations in Φ_{nm} that are much larger than 2π , such that the phase in the second term of Eq. (15) averages to zero within that frequency bin. A related possibility is if the

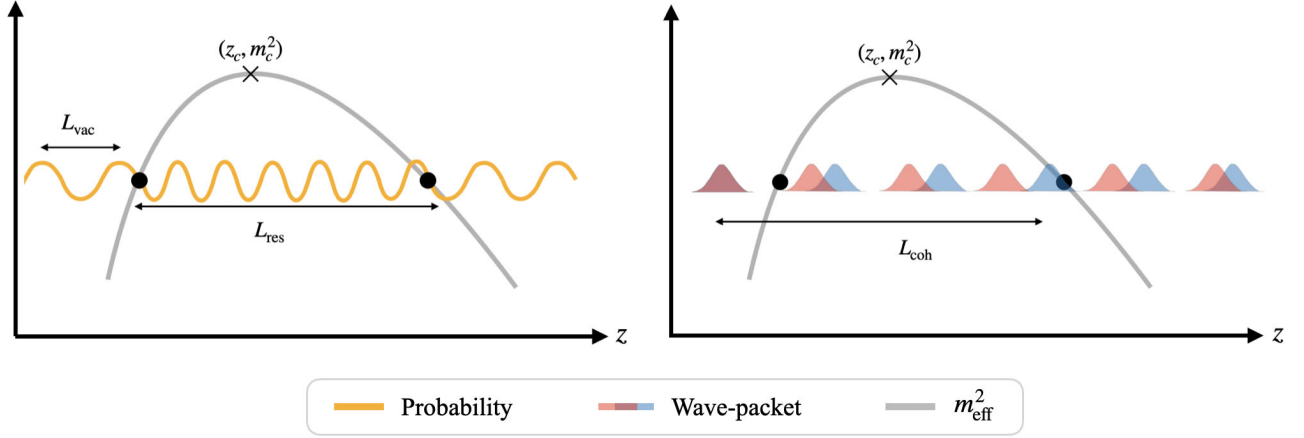


FIG. 1. A schematic representation of a peaked m_{eff} -profile (gray line) with the distance L_{res} between the resonances (black dots) marked for a specific dark photon mass. The critical point is marked by the black “ \times ” at the top of the potential. Left: A depiction of how the conversion probability oscillates spatially, where L_{vac} is the relevant conversion length scale in vacuum. Right: Propagating photon and dark photon wave packets are depicted in red and blue, respectively, for the two mass eigenstates, with the coherence length L_{coh} also shown.

spatial profile of $m_{\text{eff}}(z)$ varies between slightly different lines of sight within the angular resolution of the detector. Again, in the limit where the total acquired phase is large, small variations in the $m_{\text{eff}}(z)$ profile can lead to large phase variations within the resolution of the detector. This would potentially cause phase effects to average to zero within an angular bin, depending on the underlying spatial distribution of m_{eff} .

An additional factor in the loss of phase information is the coherence length, which determines the ability to maintain phase coherence between different mass eigenstates. This length is the distance over which wave packets of different mass eigenstates separate by a distance greater than the wave packet width, and its dependence on the production process has been investigated extensively in the context of neutrinos [31,32]. If the distance between resonance regions exceeds the coherence length, then different mass eigenstates decohere before reaching the subsequent resonance region, leading to the loss of phase information. For the purposes of this work, we assume that the states remain coherent, as we are working with relativistic DPs and do not assume that the source of SM photons or DPs is spatially or temporally localized; we will revisit these assumptions and their relevance to astrophysical environments in future work.

In the literature, phase effects are often assumed to average to zero. Ignoring the corresponding cross terms in Eq. (15), the conversion probability reduces to the standard LZ result [26,27] for a nonadiabatic two-level transition,

$$P_{A_a \leftrightarrow A_s}^{\text{LZ}} \simeq \epsilon^2 \sum_n A_n. \quad (19)$$

Note that this approximation is valid only when the above expression remains less than unity, which would otherwise seemingly violate unitarity. In this work, we always deal

with conversion probabilities $P_{A_a \leftrightarrow A_s} \ll 1$ such that multiple sequential conversions are highly suppressed.

C. Breakdown of Landau-Zener

If $m_{A'}$ happens to be near a local extremum of $m_{\text{eff}}(z)$, there exists a pair of resonant points $z_{1,2}$ such that $z_1 \lesssim z_c \lesssim z_2$ and $z_1 \simeq z_2 \simeq z_c$ (see Fig. 1). For a particular value of $m_{A'}$, such points coalesce near the position of the extremum, z_c . We refer to this mass $m_{A'} = m_{\text{eff}}(z_c) \equiv m_c$ as the *critical mass*. At this critical point z_c , the first two derivatives of $\Phi(z)$ both vanish due to the resonance appearing at the extremum of the m_{eff} potential. Near z_c , the contributions from the saddle points $A_n \propto |\Phi''(z_n)|^{-1}$ in Eq. (15) diverge. As a result, neither Eq. (15) or the LZ approximation in Eq. (19) are valid for $m_{A'} \simeq m_c$.

Instead, analytically determining the transition probability when $m_{A'} \simeq m_c$ requires incorporating the cubic term in the Taylor expansion of $\Phi(z)$ around z_c in Eq. (13), since $\Phi'(z_c) = \Phi''(z_c) = 0$. We therefore define a dimensionless variable

$$\xi \equiv \min_{z_n} \frac{|\Phi''(z_n)|}{|\Phi'''(z_n)|^{\frac{2}{3}}} \quad (20)$$

that quantifies the relative contribution of the quadratic term over the cubic term in the Taylor expansion. Hence, for $\xi \ll 1$ (near the critical mass) the quadratic term becomes negligible and one should include $\Phi'''(z_c)$ in order to accurately evaluate the conversion probability near the critical mass. We expand the phase function $\Phi(z)$ to cubic order

$$\Phi(z) \simeq \Phi(z_c) + \Phi'(z_c)(z - z_c) + \frac{1}{3!} \sigma_c |\Phi'''(z_c)| (z - z_c)^3 \quad (21)$$

with $\sigma_c = \text{sign}[\Phi'''(z_c)]$ and $\Delta_{A'}(z)$ to linear order

$$\Delta_{A'}(z) \simeq \Delta_{A'}(z_c) + \Delta_{A'}'(z_c)(z - z_c). \quad (22)$$

Incorporating these expansions and changing the integration variable to $u = \sigma_c(|\Phi'''(z_c)|/2)^{1/3}(z - z_c)$, we can then rewrite Eq. (13) as

$$P_{A_s \leftrightarrow A_s} \simeq \epsilon^2 \left| \left(\frac{2}{|\Phi''''|} \right)^{1/3} \int du \left(\Delta_{A'}(z_c) + \sigma_c \left(\frac{2}{|\Phi''''|} \right)^{1/3} u \Delta_{A'}'(z_c) \right) e^{i(\xi u + \frac{1}{3}u^3)} \right|^2, \quad (23)$$

where $\xi \equiv \sigma_c(2/|\Phi''''|)^{1/3}\Phi'$. We can then express the integrals in terms of Airy functions,

$$\begin{aligned} 2\pi \text{Ai}(x) &= \int e^{i(xu + \frac{1}{3}u^3)} du \\ 2\pi \text{Ai}'(x) &= i \int u e^{i(xu + \frac{1}{3}u^3)} du. \end{aligned} \quad (24)$$

Using Eq. (24) in Eq. (23), we obtain the conversion probability for two ‘‘coalescing saddle points’’ [33,34]

$$P_{A_s \leftrightarrow A_s} \simeq 4\pi^2 \epsilon^2 \Delta_{A'}^2 \left(\frac{2}{|\Phi''''|} \right)^{2/3} \left[\text{Ai}(-\xi) + i\sigma_c \left(\frac{2}{|\Phi''''|} \right)^{1/3} \times \left(\frac{\Delta_{A'}'}{\Delta_{A'}} - \frac{1}{6} \frac{\Phi'''''}{\Phi''''} \right) \text{Ai}'(-\xi) \right]^2 \Big|_{z_c} \quad (25)$$

which is a key result of this work and is only valid for values of $m_{A'} \simeq m_c$ such that $\xi \lesssim 1$. In Eq. (25), the entire expression is evaluated at the critical point z_c . We note that this formula is valid for two resonant crossings near an extremum; incorporating additional resonance points is possible with the approximations of Ref. [34].

III. NONMONOTONIC TOY POTENTIAL

In this section, we begin to quantify the degree to which various treatments of DP-SM photon transition probabilities can differ. Motivated by the form of the Taylor expansion of m_{eff} about its extremum, we consider the following quadratic toy model for the potential,

$$m_{\text{eff}}^2(z) = m_c^2 \left[1 - \left(\frac{z}{z_c} - 1 \right)^2 \right], \quad (26)$$

where we have chosen to take the width of the peak near z_c to be $\mathcal{O}(z_c)$ so that there is only one relevant length scale in the problem. For $m_{A'} < m_c$, there are two resonant level crossings where $m_{A'} = m_{\text{eff}}$. Because any potential will take a similar quadratic form near its extremum, we can use this toy model as a proxy to gain intuition for potentials in astrophysical systems, such as the ones discussed in the

next section. Conversion probabilities using Eq. (26) computed with different methods are shown in Fig. 2 as a function of

$$\delta m \equiv (m_c - m_{A'})/m_c. \quad (27)$$

As can be seen in the left panel of Fig. 2, when $m_{A'}$ is far from the critical mass m_c , the approximation in Eq. (15) (labelled ‘‘phase effects’’) matches well with the numerical evaluation of Eq. (13) (labeled ‘‘numerical’’). In this case, the standard LZ result of Eq. (19) (labelled ‘‘LZ’’) accurately captures the typical value of the transition probability, averaged over the oscillatory features with varying $m_{A'}$. As $m_{A'}$ approaches m_{eff} from below, the two resonance points converge spatially, eventually merging at the critical point when $\delta m = 0$, corresponding to $\xi \rightarrow 0$ in Eq. (20). As discussed in the previous section, the approximations detailed in Eqs. (15) and (19) are no longer valid for $\xi \lesssim 1$ (left of the vertical dashed line). Nevertheless, our approximation in Eq. (25) (labeled ‘‘our approx.’’) remains accurate and proves to be a reliable method of tracking the conversion probability near this critical mass. We emphasize that these approximations are substantially faster to evaluate numerically as compared with the full numerical solution of the Schrödinger equation, primarily due to the oscillatory nature of $\Phi(z)$.

In-medium resonances significantly amplify the conversion probability with respect to the vacuum value of Eq. (14). To encapsulate the enhancement due to such in-medium resonances, we first note that Eq. (16) can be rewritten as $A_n = 2\pi\mu_n$, where we have introduced a dimensionless resonance enhancement parameter

$$\mu_n = |\Delta_{A'}(z_n)| \times \left| \frac{d}{dz} \log |\Delta(z_n)| \right|^{-1} \quad (28)$$

that is analogous to the adiabaticity parameter of Keldysh in Ref. [35]. Since $P_{A_s \leftrightarrow A_s} \sim \epsilon^2 \max A_n$ in the LZ approximation, $\mu \equiv \max \mu_n$ effectively quantifies the degree that any such resonance enhances the conversion probability over the vacuum value. Hence, for $\mu \ll 1$, we expect the in-medium modifications to the transition probability to be suppressed, such that $P_{A_s \leftrightarrow A_s}$ approaches the vacuum value of Eq. (14).

This form of the resonance enhancement parameter μ is to be expected. To see this, note that for a nonmonotonic potential, such as the one of Eq. (26), $\mu_n \sim L_{\text{res}}/L_{\text{vac}}$, where L_{res} is the separation between z_n and a nearby resonant point, and $L_{\text{vac}} \sim 1/\Delta_{A'}$ is the vacuum oscillation length. Hence, for $\mu \ll 1$, the potential as seen by the DP undergoes a spatially abrupt change compared to the oscillation length, resulting in an extremely nonadiabatic transition where it is valid to use the ‘‘sudden approximation’’. Since by the uncertainty relation the DP can only resolve length scales greater than $1/\Delta_{A'} \sim L_{\text{vac}}$ for a momentum

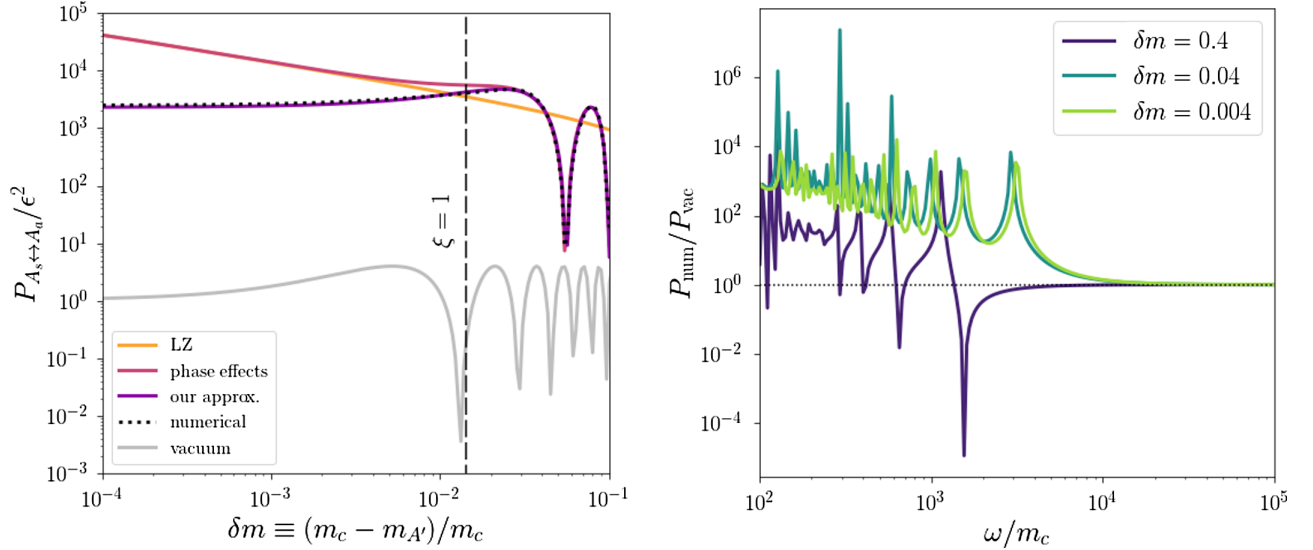


FIG. 2. Left: The conversion probability $P_{A_s \leftrightarrow A_a}$ as a function of δm (a dimensionless measure of the proximity of $m_{A'}$ to the critical mass m_c) for the toy potential of Eq. (26) with $m_c z_c = 2 \times 10^4$, $\omega / m_c = 10^2$, and $\omega z_c = 2 \times 10^6$. The region to the left of the dashed vertical line corresponds to $\xi \lesssim 1$ [see Eq. (20)], indicating the expected breakdown of standard approximations. The various approximations, consisting of the LZ result of Eq. (19), adding the term that captures phase effects in Eq. (15), and our approximation in Eq. (25), are compared to a numerical evaluation of Eq. (13) and the vacuum conversion probability of Eq. (14). Right: The ratio between the full conversion probability computed numerically and the vacuum oscillation probability as a function of ω / m_c for fixed $m_c z_c = 2 \times 10^4$ and for different values of δm . For larger frequencies, the conversion probability reduces to its vacuum value as the transition becomes increasingly nonadiabatic.

difference between active and sterile states of $\delta k = \Delta_{A'}$, it cannot effectively discern the presence of the potential over a distance of $L_{res} \ll L_{vac}$. Conversely, for $\mu \gg 1$, the potential varies over long distances compared to the vacuum oscillation length, indicating a need to account for m_{eff} using one of the other approximations detailed in the previous section.

The validity of the sudden approximation (i.e., using the vacuum transition probability) for $\mu \ll 1$ is verified numerically in the right panel of Fig. 2, which compares numerical evaluations of $P_{A_s \leftrightarrow A_a}$ with Eq. (13) to the vacuum value in Eq. (14), as a function of ω (expressed in terms of the dimensionless quantity ω / m_c) and for various representative choices of the DP mass in the form of δm . As ω increases, the vacuum oscillation length also increases compared to the effective width of the m_{eff} profile, such that the conversion probability progressively approaches its vacuum value.

IV. ASTROPHYSICAL AND COSMOLOGICAL ENVIRONMENTS

In this section, we provide a few relevant examples of environments with nonmonotonic effective photon masses where it is necessary to use Eq. (25) in order to accurately evaluate the DP conversion probability near the critical mass. It may be necessary to update some astrophysical and cosmological bounds on DPs for particular DP masses in light of these considerations.

A. Neutron star magnetospheres

Among astrophysical environments, neutron star (NS) magnetospheres are the most extreme in their variations in free charge density and electromagnetic field strength; they therefore pose an environment where m_{eff}^2 can vary substantially, affecting conversion of DPs to SM photons [36]. In particular, the rotating magnetic fields source electric fields that exert forces much larger than the gravitational binding energy on the NS surface charges. As a result, charges are pulled off of the surface and fill the magnetosphere of the NS. The charges then redistribute themselves in a way such that the Lorentz force on them cancels, producing a corotating plasma surrounding the NS. The charge density of this plasma can be approximated by the Goldreich-Julian model [37], which has been generalized to account for relativistic effects [38]

$$n_e^{GJ}(r, \theta) = \frac{2\mathbf{\Omega} \cdot \mathbf{B}}{e} [F_1(\bar{r}) \sin^2 \theta - F_2(\bar{r})(\sin^2 \theta - 2 \cos^2 \theta)]. \quad (29)$$

Here, r and θ are polar coordinates such that r is the distance from the center of the NS, θ is the polar angle with respect to the NS's rotation axis $\hat{\mathbf{\Omega}}$, \mathbf{B} is the magnetic field outside the NS (assumed to be dominated by its dipole component), and $\mathbf{\Omega}$ is the rotational frequency. The functions

$$F_1(\bar{r}) = \bar{r}^3 \left\{ \left(1 - \frac{\beta}{\bar{r}^3} \right) \left[\frac{2}{\bar{r}-1} - \frac{1}{(\bar{r}-1)^2} + 2 \ln \left(1 - \frac{1}{\bar{r}} \right) \right] \right\} \\ + \left(2 + \frac{\beta}{\bar{r}^3} \right) \left\{ \frac{1}{\bar{r}} + \frac{1}{\bar{r}-1} + 2 \ln \left(1 - \frac{1}{\bar{r}} \right) \right\} \quad (30)$$

and

$$F_2(\bar{r}) = \bar{r}^3 \frac{2(1-\frac{\beta}{\bar{r}^3})}{1-\frac{1}{\bar{r}}} \left\{ \frac{1}{2\bar{r}^2} + \frac{1}{\bar{r}} + \ln \left(1 - \frac{1}{\bar{r}} \right) \right\} \quad (31)$$

incorporate relativistic corrections, where we have defined $\bar{r} = r/r_g$ and $\beta = 2/5(r_{\text{NS}}/r_g)^2$ for a NS of radius r_{NS} and Schwarzschild radius of r_g . Note that at large distances, $\lim_{\bar{r} \rightarrow \infty} F_1(\bar{r}) = -1/2\bar{r}$ and $\lim_{\bar{r} \rightarrow \infty} F_2(\bar{r}) = -2/3$.

Following Ref. [39], we take the rotation axis to be aligned with $\hat{\mathbf{z}}$, such that

$$\boldsymbol{\Omega} \cdot \mathbf{B} = \frac{B_0}{2r_{\text{LC}}} \left(\frac{r_{\text{NS}}}{r} \right)^3 [3 \cos \theta \hat{\mathbf{m}} \cdot \hat{\mathbf{r}} - \cos \alpha_B] \quad (32)$$

and

$$\hat{\mathbf{m}} \cdot \hat{\mathbf{r}} = \cos \theta \cos \alpha_B + \sin \theta \sin \alpha_B \cos(\Omega t), \quad (33)$$

where B_0 is the magnetic field strength at the NS surface, α_B is the orientation angle of the magnetic field with respect to the rotation axis, and $r_{\text{LC}} = 1/\Omega$ is the light-cylinder radius.

In the presence of large magnetic fields (with $B_0 \sim B_c$ where $B_c = m_e^2/e$ is the critical value of the magnetic field), both the magnetic field and the plasma contribute to m_{eff}^2 for the propagating photon mode (that has its electric field parallel to the plane containing the propagation and NS magnetic field vectors) but with opposite signs [36,40,41]. We can decompose the effective SM photon mass as $m_{\text{eff}}^2 = V_B + V_{\text{pl}}$, where

$$V_B \simeq -\frac{7\alpha}{45\pi} b^2 \hat{q}_B \omega^2 \sin^2 \theta, \quad V_{\text{pl}} = \omega_p^2 \sin^2 \theta, \quad (34)$$

$b = B(r)/B_c$, $\omega_{\text{pl}}^2 = 4\pi\alpha n_e^{\text{GJ}}/m_e$ is the plasma frequency, and \hat{q}_B is a fitting function that reproduces the correct $b \ll 1$ and $b \gg 1$ behavior [41]

$$\hat{q}_B \equiv \frac{1 + 1.2b}{1 + 1.33b + 0.56b^2}. \quad (35)$$

The frequency-dependent B -field contribution to the photon potential V_B originates from nonlinear vacuum polarization effects (analogous to the Euler-Heisenberg term in pure QED) and contributes effectively only when $B(r) \gtrsim B_c$. The opposing signs of V_B and V_{pl} give rise to a nonmonotonic profile for $m_{\text{eff}}^2(r)$. Note that the potential is nonmonotonic regardless of the inclusion of relativistic corrections in Eq. (29).

The exact form of the SM photon potential $m_{\text{eff}}^2(r)$ is sensitive to various NS parameters, such as the magnetic field strength, rotation speed, and frequency ω , resulting in a wide range of possible profiles. Since the electron density and magnetic field both scale as $\propto 1/r^3$ far from the NS's surface, the potentials of Eq. (34) scale as $V_B \propto -r^{-6}$ and $V_{\text{pl}} \propto r^{-3}$. As a result, $m_{\text{eff}}^2 < 0$ when V_B dominates at intermediate distances (which precludes the possibility of a resonance in this region) and $m_{\text{eff}}^2 > 0$ when V_{pl} dominates at large distances. Hence, the potential reaches its extremum at the turnover point r_c when $V_{\text{pl}}(r_c) \sim -V_B(r_c)$. For $B_0 \lesssim B_c$, the corresponding critical radius and mass take simple analytical forms,

$$r_c \sim (\omega^2 r_{\text{LC}} B_0)^{1/3} \frac{e r_{\text{NS}}}{m_e}, \quad m_c \sim \frac{m_e}{e \omega r_{\text{LC}}}. \quad (36)$$

As discussed in Sec. II C, when the dark photon is close to but slightly less than the critical mass, there exist two nearby resonant points $r_1 \simeq r_2$ such that $r_1 \lesssim r_c \lesssim r_2$. These resonances are physically realized only if the critical radius r_c lies in the range $r_{\text{NS}} \leq r_c \leq r_{\text{LC}}$, which is equivalent to

$$\frac{r_{\text{NS}}^2}{r_{\text{LC}}} \lesssim \frac{e^2 B_0}{m_e B_c} \omega^2 \lesssim \frac{r_{\text{LC}}^2}{r_{\text{NS}}}. \quad (37)$$

The left panel of Fig. 3 shows that the critical mass m_c spans many orders of magnitude for a representative range of possible values for the light-cylinder radius r_{LC} and frequency ω , fixing $B_0/B_c = 10$ and using the full form for the potential m_{eff}^2 . In the right panel, we show the conversion probability as a function of δm , using the various approximations discussed in Sec. II, for a particular choice of NS parameters. By comparing to Fig. 2, we note that our findings qualitatively resemble the probabilities for the toy example of the previous section, further illustrating that Eq. (25) is required to accurately compute $P_{A_a \leftrightarrow A_s}$ for $\delta m \ll 1$.

B. Intergalactic medium

The free electron fraction of the intergalactic medium (IGM) has fluctuated considerably since recombination, diminishing during the dark ages and cosmic dawn before increasing again during reionization, all while the density of the Universe was redshifting as $\sim (1+z)^3$. As a result, cosmic microwave background (CMB) photons experience large variations in their effective mass as they traverse the IGM,

$$m_{\text{eff}}^2 \simeq \omega_{p,e}^2 - (\omega/Ry)^2 \omega_{p,\text{HI}}^2, \quad (38)$$

where $\omega_{p,e} = \sqrt{4\pi\alpha n_e/m_e}$ and $\omega_{p,\text{HI}} = \sqrt{4\pi\alpha n_{\text{HI}}/m_e}$ are contributions to the plasma frequency from the average number density of free electrons n_e and electrons bound in

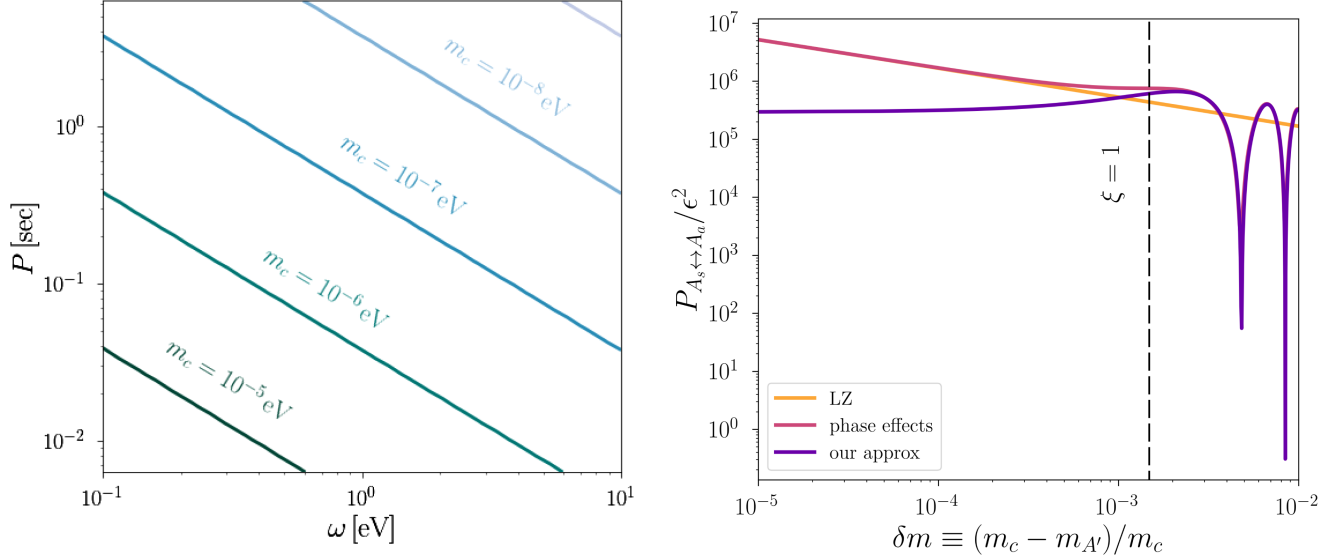


FIG. 3. Left: Contours of the critical mass m_c in the environment of a neutron star, in the plane spanned by the rotation period P of the NS and frequency ω for a fixed value of the magnetic field $B_0/B_c = 10$. The critical mass varies considerably for fixed neutron star properties, meaning that any conversion processes occurring over a range of frequencies would only be accurately described by the approximations developed in this work. Right: As in Fig. 2, but for the neutron star potential of Eq. (34) with $r_{LC} = 300$ km, $B_0/B_c = 10$, and $\omega = 0.08$ eV. The similarity of this behavior with that of the toy model underscores the necessity of using the approximation near the critical mass.

neutral hydrogen n_{HI} , respectively. As shown in the top-left panel of Fig. 4, the resulting SM photon potential has two local extrema independent of frequency near $z \sim 10$, corresponding to just before and after reionization, as well as additional local maxima for frequencies significantly larger than the CMB blackbody temperature, i.e., $\omega/T \gtrsim \text{few}$ [17,42]. The corresponding values of the critical mass are roughly $m_c \sim \text{few} \times 10^{-13}$ eV, $m_c \sim 10^{-14}$ eV, and $m_c \sim 10^{-11}$ eV $\times (T/\omega)^2$. We note that the first two of these are subject to uncertainties in the ionization history. We postpone a more careful consideration of alternative parametrizations of reionization [43] as well as the incorporation of fluctuations in the plasma density (along the lines of Refs. [18,19]) to future study.

Previous studies have derived strong constraints on DPs from requiring that the CMB spectrum remains a blackbody, as resonant conversion from CMB photons to DPs could induce observable spectral distortions in the frequency range probed by the Far InfraRed Absolute Spectrophotometer (FIRAS) [45]. Accounting for both the mean value and fluctuations of the plasma density has led to strong constraints at the level of $\epsilon \lesssim 10^{-7}$ for 10^{-15} eV $\lesssim m_{A'} \lesssim 10^{-6}$ eV [17–19,21]. Such studies have employed the LZ approximation discussed above, but this is expected to break down for $m_{A'} \simeq m_c$, necessitating the use of Eq. (25). This is demonstrated in the top-right panel of Fig. 4, which shows the conversion probability for DP masses near the critical point as computed using different approximation schemes, analogous to the toy example of Fig. 2. Given the form of the mean photon potential

(i.e., ignoring plasma density fluctuations), DPs with 10^{-13} eV $\lesssim m_{A'} \lesssim 10^{-14}$ eV have three or more resonance points, with two critical points occurring around the time of reionization. It is noteworthy that both $\omega(t)$ and $\Phi''(t)$ decrease steeply with the age of the Universe, meaning that resonances that occur later are more adiabatic. As a result of the $\sim 1/(\omega^2 \Phi'')$ scaling of the A_n in Eq. (16), resonances occurring at later times therefore have a much greater contribution to the total conversion probability as computed with the LZ formalism of Eq. (19). We therefore ignore the earliest level crossings that occur well before reionization in computing the conversion probability and include only the ones occurring around the time of reionization.

The conversion probability fluctuates sharply as a function ω and m_{eff} due to the phase effects discussed in Sec. II B. Effects from variations in ω are potentially observable depending on the frequency resolution of the detector, which is shown for FIRAS as the vertical gray region in the bottom row of Fig. 4. Variations in m_{eff} arise from the fact that different lines of sight trace slightly different ionization histories due to the patchy morphology of reionization, leading to shifts in the SM photon potential and conversion probability along slightly different lines of sight. We note that this opens the possibility for the constraints on DPs from CMB spectral distortions to form more of a “fog” (due to theoretical uncertainties in computing the conversion probabilities) rather than a sharp exclusion boundary in parameter space. We leave the question of whether or not these variations average out across different lines of sight to future work.

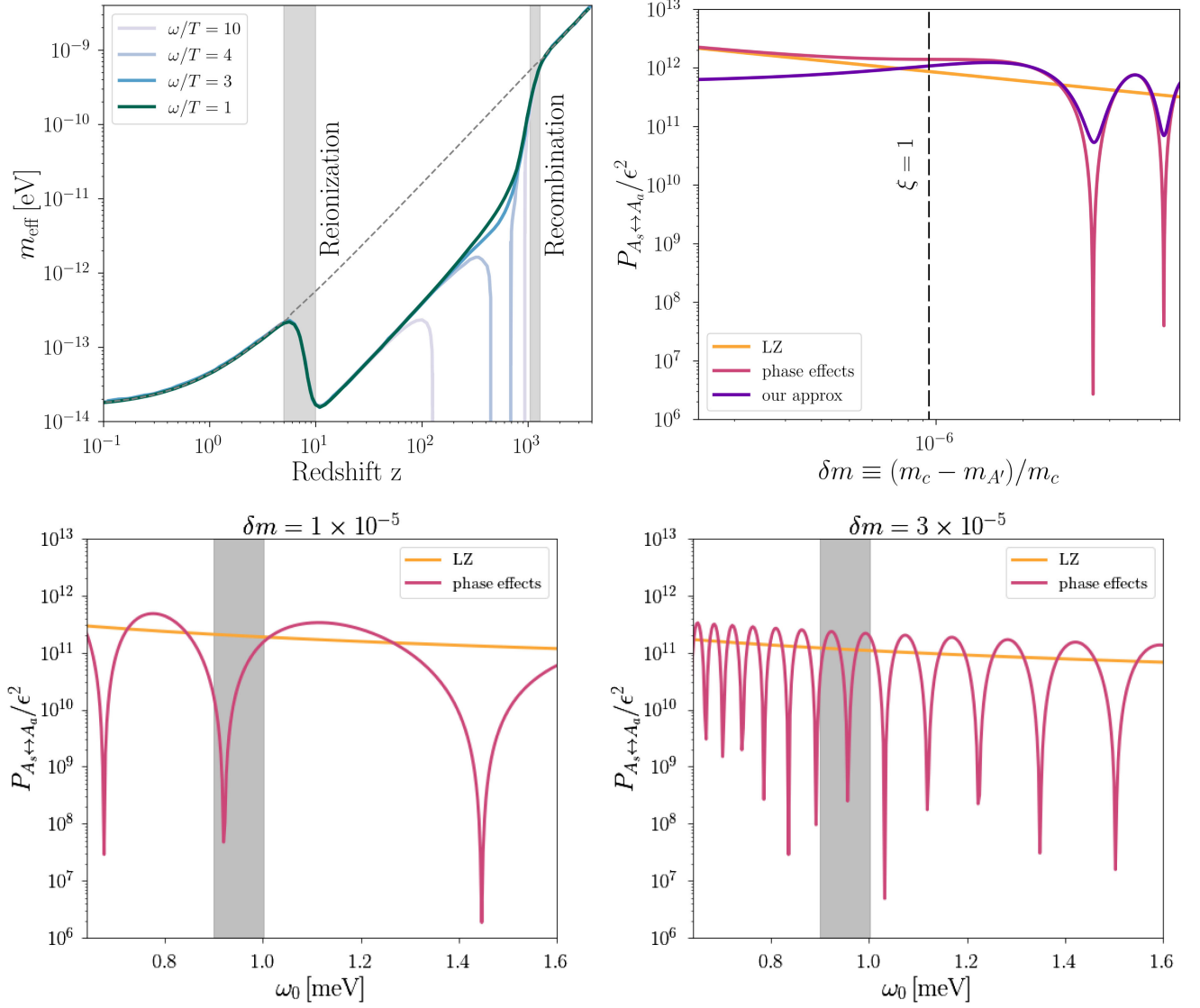


FIG. 4. Top left: The spatially averaged evolution of m_{eff} in the intergalactic medium as a function of redshift for different frequencies. Reionization induces extrema in the potential experienced by CMB photons. Top right: As in Fig. 2, but for the IGM potential shown in the top-left panel for a frequency of $\omega = 7 \times 10^{-4}$ eV and $m_c \simeq 2.5 \times 10^{-13}$ eV. Bottom: As in Fig. 2, but with two values of fixed dark photon masses and instead varying the frequency. Also shown as a gray vertical band is the frequency resolution of FIRAS, 24.6 GHz [44]. For values of the dark photon mass near the critical mass, the frequency oscillations do not necessarily average out within the frequency resolution of the instrument, meaning that phase effects are potentially significant in determining the observed conversion probability. Note that in the bottom panels, the values of δm correspond to $\xi > 1$ where we expect our approximation is not necessary to compute the conversion probability.

We also note that these considerations may be relevant for the dark screening effect that was recently proposed in Ref. [46], since there the photons passing through halos containing a gas overdensity will have two resonance points near the maximum plasma frequency.

C. Solar chromosphere

In stellar chromospheres, the density of free electrons n_e^c exhibits a distinct peak located approximately 10^3 km above the photosphere, as depicted in Fig. 5 [47]. This non-monotonic electron density translates to a nonmonotonic

$m_{\text{eff}}^2 = 4\pi\alpha(n_e^c)^2/m_e$. Additionally, the form of the profile yields a small value of ξ for a wide range of frequencies if the DP mass is near the critical mass. For instance, for $\delta m \sim 0.01$, $\xi \lesssim 1$ for $\omega \gtrsim 0.1$ eV. This implies the unavoidable need for the approximation of Eq. (25) to accurately assess the conversion probability shown in Fig. 5. This may be important to incorporate for DP searches involving the Sun, for instance strategies that could complement existing searches involving resonant level crossing in the solar atmosphere (e.g., Refs. [48,49]). We explore this possibility in future work.

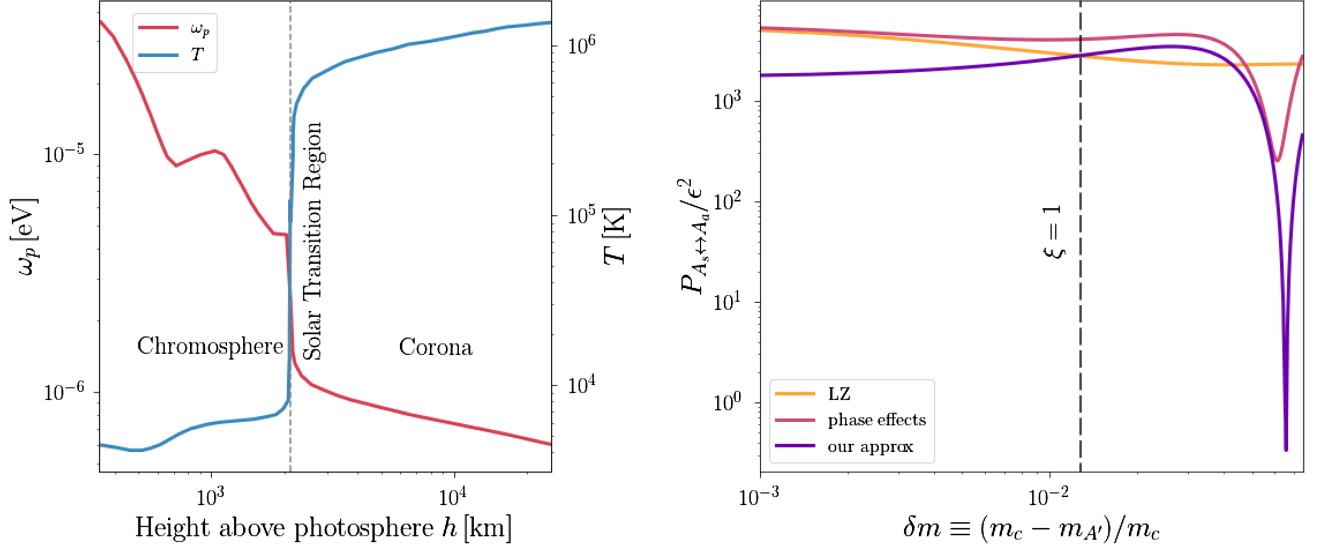


FIG. 5. Left: The nonmonotonic plasma frequency ω_p and temperature T profile above the solar photosphere. The solar transition region which separates the chromosphere and corona is also shown. Right: As in Fig. 2, but with the chromospheric potential depicted in the left panel.

V. CONCLUSION

In this paper, we have developed an accurate approximation for the solution to the Schrödinger equation for a two-state system (specifically, photons and dark photons) with multiple nearby resonances about the extremum of a potential. This approximation can be viewed as an extension of the LZ formula, which is widely used for computing the transition probability between photons and dark photons. Using a toy model, we find that there can be large corrections to the conversion probability for specific dark photon masses in a given potential (i.e., given some properties of the background environment that affect the propagation of photons).

We have highlighted the application of this formalism to various astrophysical systems where multiple resonances between dark photons and photons are possible. Some of these systems have been previously used to constrain the existence of dark photons through their observed spectral signatures, which makes it important to quantify the effects of multiple resonances on the constraints. We have not attempted to update any of these constraints from specific astrophysical systems, and leave such an analysis to future work. We note that applying our formalism to neutron stars seems especially promising due to the large resonant enhancement factors over the vacuum conversion probability as well as the wide range of possible values of the critical mass.

There are several additional subtleties in the conversion between photons and dark photons that we have not considered here, such as the role of decoherence between

different states, which may be particularly relevant when the dark photon is nonrelativistic (e.g., in the case of dark photon dark matter). We note that much of the formalism here, along with the associated subtleties, may be transferred over to axion-photon conversions and neutrino oscillations. We leave consideration of all of these effects to future work.

ACKNOWLEDGMENTS

It is a pleasure to thank Bryce Cyr, Adrian Liu, Hongwan Liu, and Anirudh Prabhu for valuable conversations and correspondence pertaining to this work. The research of N.B. was undertaken thanks in part to funding from the Canada First Research Excellence Fund through the Arthur B. McDonald Canadian Astroparticle Physics Research Institute. N.B. and K.S. acknowledge support from a Natural Sciences and Engineering Research Council of Canada Subatomic Physics Discovery Grant and from the Canada Research Chairs program. A.B. is supported by the U.S. Department of Energy, Office of Science, National Quantum Information Science Research Centers, Superconducting Quantum Materials and Systems Center (SQMS) under Contract No. DE-AC02-07CH11359. Fermilab is operated by the Fermi Research Alliance, LLC under Contract No. DE-AC02-07CH11359 with the U.S. Department of Energy. Research at Perimeter Institute is supported in part by the Government of Canada through the Department of Innovation, Science and Economic Development Canada and by the Province of Ontario through the Ministry of Colleges and Universities.

- [1] B. Holdom, *Phys. Lett.* **166B**, 196 (1986).
- [2] K. R. Dienes, C. F. Kolda, and J. March-Russell, *Nucl. Phys.* **B492**, 104 (1997).
- [3] S. A. Abel and B. W. Schofield, *Nucl. Phys.* **B685**, 150 (2004).
- [4] B. Batell and T. Gherghetta, *Phys. Rev. D* **73**, 045016 (2006).
- [5] G. Aldazabal, L. E. Ibanez, F. Quevedo, and A. M. Uranga, *J. High Energy Phys.* 08 (2000) 002.
- [6] S. Abel and J. Santiago, *J. Phys. G* **30**, R83 (2004).
- [7] S. A. Abel, M. D. Goodsell, J. Jaeckel, V. V. Khoze, and A. Ringwald, *J. High Energy Phys.* 07 (2008) 124.
- [8] B. S. Acharya, S. A. R. Ellis, G. L. Kane, B. D. Nelson, and M. J. Perry, *Phys. Rev. Lett.* **117**, 181802 (2016).
- [9] B. S. Acharya, S. A. R. Ellis, G. L. Kane, B. D. Nelson, and M. Perry, *J. High Energy Phys.* 09 (2018) 130.
- [10] T. Gherghetta, J. Kersten, K. Olive, and M. Pospelov, *Phys. Rev. D* **100**, 095001 (2019).
- [11] N. Arkani-Hamed and N. Weiner, *J. High Energy Phys.* 12 (2008) 104.
- [12] E. Fischbach, H. Kloor, R. A. Langel, A. T. Y. Liu, and M. Peredo, *Phys. Rev. Lett.* **73**, 514 (1994).
- [13] N. Vinyoles, A. Serenelli, F. Villante, S. Basu, J. Redondo, and J. Isern, *J. Cosmol. Astropart. Phys.* 10 (2015) 015.
- [14] J. Redondo and G. Raffelt, *J. Cosmol. Astropart. Phys.* 08 (2013) 034.
- [15] H. An, M. Pospelov, and J. Pradler, *Phys. Lett. B* **725**, 190 (2013).
- [16] S. D. McDermott and S. J. Witte, *Phys. Rev. D* **101**, 063030 (2020).
- [17] A. Mirizzi, J. Redondo, and G. Sigl, *J. Cosmol. Astropart. Phys.* 03 (2009) 026.
- [18] A. Caputo, H. Liu, S. Mishra-Sharma, and J. T. Ruderman, *Phys. Rev. Lett.* **125**, 221303 (2020).
- [19] A. Caputo, H. Liu, S. Mishra-Sharma, and J. T. Ruderman, *Phys. Rev. D* **102**, 103533 (2020).
- [20] S.-P. Li and X.-J. Xu, *J. Cosmol. Astropart. Phys.* 09 (2023) 009.
- [21] A. A. Garcia, K. Bondarenko, S. Ploekinger, J. Pradler, and A. Sokolenko, *J. Cosmol. Astropart. Phys.* 10 (2020) 011.
- [22] J. I. Kapusta and C. Gale, *Finite-Temperature Field Theory: Principles and Applications* (Cambridge University Press, Cambridge, England, 2006).
- [23] W. Heisenberg and H. Euler, *Z. Phys.* **98**, 714 (1936).
- [24] A. Berlin, J. A. Dror, X. Gan, and J. T. Ruderman, *J. High Energy Phys.* 05 (2023) 046.
- [25] A. Berlin, R. Tito D’Agnolo, S. A. R. Ellis, and J. I. Radkovski, *J. High Energy Phys.* 08 (2023) 017.
- [26] C. Zener, *Proc. R. Soc. A* **137**, 696 (1932).
- [27] L. D. Landau, *Phys. Z. Sowjetunion* **2**, 46 (1932).
- [28] G. Raffelt and L. Stodolsky, *Phys. Rev. D* **37**, 1237 (1988).
- [29] L. Wolfenstein, *Phys. Rev. D* **17**, 2369 (1978).
- [30] S. P. Mikheyev and A. Y. Smirnov, *Sov. J. Nucl. Phys.* **42**, 913 (1985).
- [31] S. Nussinov, *Phys. Lett.* **63B**, 201 (1976).
- [32] H. Anada and H. Nishimura, *Phys. Rev. D* **41**, 2379 (1990).
- [33] J. Connor and R. Marcus, *J. Chem. Phys.* **55**, 5636 (1971).
- [34] R. Beuc, M. Movre, and B. Horvatić, *Atoms* **7**, 47 (2019).
- [35] L. V. Keldysh, *J. Exp. Theor. Phys.* **20**, 1307 (1965).
- [36] J.-F. Fortin and K. Sinha, *J. Cosmol. Astropart. Phys.* 11 (2019) 020.
- [37] P. Goldreich and W. H. Julian, *Astrophys. J.* **157**, 869 (1969).
- [38] U. A. Mofiz and B. J. Ahmedov, *Astrophys. J.* **542**, 484 (2000).
- [39] A. Hook, Y. Kahn, B. R. Safdi, and Z. Sun, *Phys. Rev. Lett.* **121**, 241102 (2018).
- [40] D. Lai and W. C. G. Ho, *Astrophys. J.* **566**, 373 (2002).
- [41] A. Y. Potekhin, D. Lai, G. Chabrier, and W. C. G. Ho, *Astrophys. J.* **612**, 1034 (2004).
- [42] S. Seager, D. D. Sasselov, and D. Scott, *Astrophys. J. Lett.* **523**, L1 (1999).
- [43] B. Greig and A. Mesinger, *Mon. Not. R. Astron. Soc.* **465**, 4838 (2017).
- [44] FIRAS data (NASA), https://lambda.gsfc.nasa.gov/product/cobe/firas_products.html.
- [45] D. J. Fixsen, E. S. Cheng, J. M. Gales, J. C. Mather, R. A. Shafer, and E. L. Wright, *Astrophys. J.* **473**, 576 (1996).
- [46] D. Pirvu, J. Huang, and M. C. Johnson, [arXiv:2307.15124](https://arxiv.org/abs/2307.15124).
- [47] M. Aschwanden, *Physics of the Solar Corona: An Introduction with Problems and Solutions* (Springer Science & Business Media, New York, 2006).
- [48] H. An, F. P. Huang, J. Liu, and W. Xue, *Phys. Rev. Lett.* **126**, 181102 (2021).
- [49] H. An, X. Chen, S. Ge, J. Liu, and Y. Luo, [arXiv:2301.03622](https://arxiv.org/abs/2301.03622).